(Received 18 December 2024, Accepted 23 January 2025, Scheduled 4 February 2025)

Low-Profile Wide Axial-Ratio BeamWidth Circularly Polarized Antenna with Simple Feed

Wen-Ying Lu, Xiao Ding*, and Wei Shao

School of Physics, University of Electronic Science and Technology of China, Chengdu 611731, China

ABSTRACT: To effectively receive circularly polarized (CP) waves at large angles, it is necessary for antennas to have large axial ratio beamwidth (ARBW). For instance, geostationary satellite receiver antennas employed in regions with high latitudes necessitate a broad ARBW. In this paper, the mechanism to broaden ARBW is analyzed, and a CP antenna with low profile is designed and fabricated. With L-shaped branches and vertical extension segments (VESs), ARBW of the proposed antenna has been effectively broadened. Moreover, compared with recently reported wide ARBW artworks, it features a simple structure and feeding mechanism. The proposed antenna within the working bandwidth (from 4.79 to 4.95 GHz, 3.3%) achieves a 3 dB ARBW of 243° in the $\varphi = 0°$ plane while the 3 dB ARBW reaches 199° in the $\varphi = 90°$ plane. The measured results agree well with the simulated ones.

1. INTRODUCTION

Circularly polarized (CP) antennas can mitigate polarization mismatch by eliminating the need for precise alignment between the transmitting antenna and receiving antenna, and can suppress multipath interference from other interfering objects on the ground and in the surrounding area. These advantages make CP antennas more and more valuable in satellite and wireless communications [1]. Nowadays, some scholars focus their research on how to improve the operating bandwidth of CP antennas while neglecting the effect of 3 dB axial-ratio beamwidth (ARBW). In satellite navigation, aircraft and other fields, to improve the quality and stability of the electronic system, the antenna is required to have a wide ARBW, which can enable the antenna to receive CP signals with the same rotation direction in a wide range of angles. For example, a 3 dB ARBW of 120° enables GPS system to receive as many satellite signals as possible anywhere on Earth [2]. The published papers primarily utilize the following methods to broaden ARBW. The use of different types of metal back cavities [2–5] to change the beam shape and spatial phase is a common approach. In [4], a sawtooth three-dimensional metal ground effectively widens ARBW from 140° to 204°. However, its structure is complex, and four ports are often required to be excited to obtain a CP wave. Another effective method is to add short-circuit pins which introduce shunt inductive effects, thereby widening ARBW from 53° to 143° [6]. It is a single-feed low-profile CP antenna, and hence the impedance bandwidth (IBW) is narrow. The third method is to add coupling strips to extend the current path [7, 8]. In [8], four L-shaped metal strips, each with a length of $\lambda_L/2$ (λ_L is the wavelength of the center frequency), are attached around the perimeter of the central circular patch. The measured results indicate that ARBW is expanded from 104° to 220° in the yoz plane. Furthermore, this antenna achieves a 55.6% IBW and 33% AR bandwidth by employing a complex sequential rotation (SR) feeding network composed of Wilkinson power dividers and wideband Schiffman phase shifters. However, its operating bandwidth drops dramatically if a dual-port feed is used instead of the four-port SR feed. It is undeniable that the SR feed networks bring certain benefits, but they can also substantially increase the complexity of the system, raise the cost and greatly increase the size of the antenna, resulting in a limit of their application range. Some researchers introduce an artificial magnetic conductor (AMC) or metasurface to improve the spatial phase stability of the antenna and thus widen ARBW [9, 10]. Ref. [9] proposes a metasurface antenna, and its E_φ and E_θ can be nearly equal in amplitude with a phase difference of 90° over a wide angle range leading to a wide 3 dB ARBW of 205°. However, it shows a large structure size. The last method is to etch slots or introduce magnetic currents [11, 12]. The antenna in [12] achieves ARBW of 226° by etching two pairs of narrow slots along the diagonal lines of the upper square patch. These two pairs of narrow slots are equivalent to two pairs of magnetic dipoles spaced a quarter wavelength apart, placed along the diagonal to provide a 90° phase difference between them. Additionally, the magnetic dipoles exhibit wide beam characteristics when they are oriented parallel to the ground, making this approach one of the primary methods to achieve the wide ARBW.

From the above analyses, it is clear that complex multiport feed is the conventional way to design wide ARBW CP antennas, but it also has some inherent drawbacks. In this paper, a low-profile wide ARBW CP antenna with a simple single-port feed is designed. This paper proposes a vertical extension segment (VES) structure which can effectively broaden the antenna ARBW. The evolutionary process of the proposed antenna is analyzed. Compared with other single-feed wide ARBW CP antennas, it has a relatively decent operating band-

* Corresponding author: Xiao Ding (xding@uestc.edu.cn).

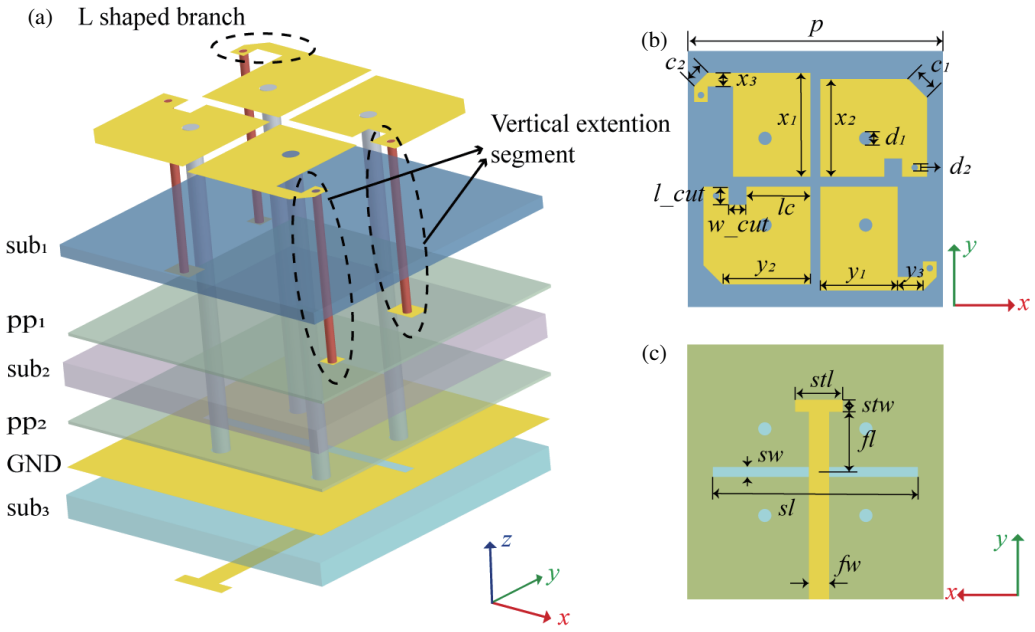

FIGURE 1. Geometry of the proposed element antenna. (a) Exploded view, (b) top view, and (c) back view. Parameters: $p = 38$, $x_1 = 15.4$, $y_1 = 11.5$, $x_2 = 14.5$, $y_2 = 13.07$, $x_3 = 2$, $y_3 = 3.8$, $c_1 = 4$, $c_2 = 2.83$, $d_1 = 2$, $d_2 = 1$, $lc = 9.5$, $w\_cut = 2.7$, $l\_cut = 2.7$, $sw = 1.5$, $sl = 30.47$, $fw = 2.97$, $fl = 9$, $stw = 1.76$, and $stl = 7.04$ (unit: mm).

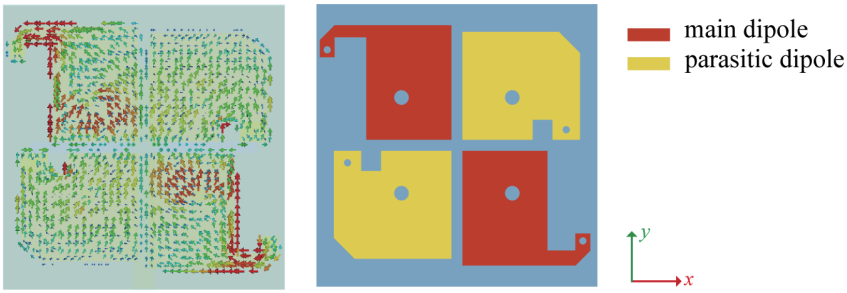

FIGURE 2. Schematic diagram of the main dipole and parasitic dipole.

width (3.34%) and excellent ARBW of 250°. On the other hand, it shows a more compact and simpler structure than the multifeed wide ARBW CP antennas reported in recent years.

2. ANTENNA DESIGN

2.1. Antenna Structure

The geometry of the proposed antenna is depicted in Fig. 1. It consists of three substrate layers, sub_1 (Rogers RT5880, $\varepsilon_r = 2.2$ and $h_1 = 0.508\,\text{mm}$), sub_2 (F4BM-2, $\varepsilon_r = 2.2$ and $h_2 = 1.6\,\text{mm}$), and sub_3 (F4BM-2, $\varepsilon_r = 2.65$ and $h_3 = 1.2\,\text{mm}$), and each two of them are connected by a prepreg (pp_1 or pp_2, $\varepsilon_r = 4.4$ and $h_{pp} = 0.07\,\text{mm}$). The proposed antenna can be seen as two pairs of crossed magneto-electric (ME) dipoles, as shown in Fig. 2. In the xoy plane, the ME dipole located in the second and fourth quadrants is the main dipole, consisting of rectangular patches and L-shaped strips made with chamfer, possessing strong current distribution and serving as the primary dipole for radiating CP waves. In the first and third quadrants, these patches are equivalent to a parasitic ME dipole used to regulate the direction of electric current and magnetic current. These parasitic patches consist of two rectangular patches with the corners cut and a notch chiseled out, as shown in Fig. 1(b). Four VESs have been added at the stubs of the both pairs of ME dipoles. The proposed antenna is fed with a coupling slot above the ground, and a stub is added at the feedline terminal to realize impedance matching as shown in Fig. 1(c).

Figure 4 presents the simulated results of proposed antenna. ARBW of the proposed antenna reaches 243° in the $\varphi = 0°$ plane and 199° in the $\varphi = 90°$ plane over the frequency range from 4.8 to 4.95 GHz. IBW of the proposed antenna is 18%, and the ARBW is 3.3%. From Table 1, it can be observed that ARBW varies with the frequency.

2.2. Vertical Extension Segment

The reason for narrow ARBW of most antennas is that the spatial phase difference of the electric field at large angles cannot meet 90°. To solve this problem, it is usually necessary to add some additional structures to compensate for the spatial phase

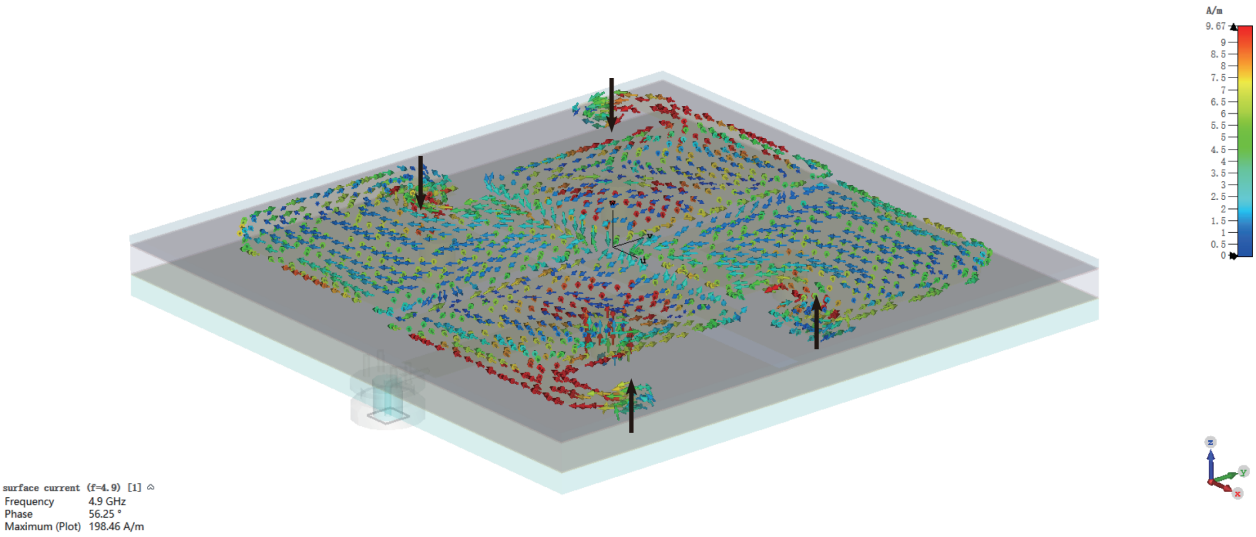

FIGURE 3. Current distribution on the patches and the vertical extension segments.

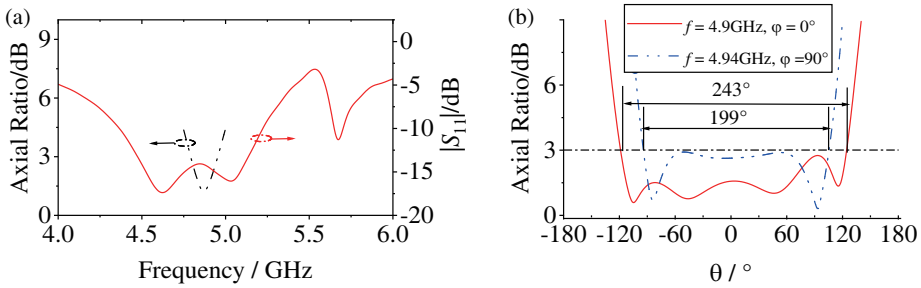

FIGURE 4. Simulated results of the proposed antenna (a) AR and $|S_{11}|$ and (b) ARBW.

TABLE 1. Simulated 3 dB AR beamwidth at different frequencies.

f/GHz	$\varphi = 0°$	$\varphi = 90°$
4.8	49° (−17° ∼ 32°)	125° (−53° ∼ 72°)
4.84	112° (−53° ∼ 59°)	166° (−76° ∼ 90°)
4.88	202° (−121° ∼ 81°)	182° (−85° ∼ 97°)
4.9	243° (−118° ∼ 125°)	189° (−89° ∼ 100°)
4.94	235° (−113° ∼ 122°)	199° (−94° ∼ 105°)
4.95	234° (−112° ∼ 122°)	48° (−24° ∼ 24°)

difference of the electric field, such as AMC and metal back cavity. This not only increases the size of the antenna but also greatly increases the complexity of the antenna structure.

The VES structure proposed in this paper can be used to improve ARBW of the antenna, and it has a simple structure without adding extra dimensions to the antenna. As can be seen from Fig. 3, due to the addition of VES, a small current in the vertical direction appears at the end of each patch (the black arrows in Fig. 3). These four vertical currents can be equivalent to four monopole antennas. The E-plane radiation pattern of an ideal monopole antenna (with an infinite ground plane) is similar to a reclining figure "8", with a null at $\theta = 0°$ and a maximum at $\theta = 90°$ [13]. When the ground plane of the monopole antenna is of a finite size, the directions of the extreme values will be slightly shifted, as shown in [14]. The radiated electric field of the vertical currents introduced by the VES structures can superimpose the original antenna's radiated electric field at large angles, thereby compensating for the degradation of ARBW at large angles. The VES structure can be utilized to enhance the ARBW of a variety of planar antennas, demonstrating good applicability.

2.3. Working Principle of Circular Polarization

A ME dipole is composed of a pair of electric dipoles and magnetic dipoles. When their far-field radiation characteristics are studied, electric dipoles can be approximated as short currents, and magnetic dipoles can be approximated as an electric small loop antenna. The far-field electric field distribution of the short currents and small loop antenna is given by:

$$\text{short current: } E_\theta = j(60\pi IL\sin\theta)/r\lambda \quad (1)$$

$$\text{small loop antenna: } E_\varphi = (120\pi^2 IA\sin\theta)/r\lambda^2 \quad (2)$$

where L is the length of the short current, I the current intensity, A the area of the small loop antenna, r the radiation distance, and λ the wavelength in the free space.

When two electric field components are mutually orthogonal, have equal amplitudes, and possess a phase difference of 90°, CP waves can be excited. It can be observed from Equations (1) and (2) that E_θ and E_φ are inherently orthogonal to each other, and due to the presence of an imaginary compo-

nent (represented by j) in E_θ, there exists a natural 90° phase difference between E_θ and E_φ. Thus, by adjusting their amplitudes to be equal, CP waves can be radiated. Based on the above, when short currents and electric small loop antenna are placed perpendicular to each other, CP waves can be radiated. Therefore, for the case of a ME dipole, by arranging the electric dipole and the equivalent magnetic dipole in parallel, a CP ME dipole is designed.

2.4. Evolution of the Proposed Antenna

The evolution process of the proposed antenna can be divided into two parts: from Ant. 1 to Ant. 4, it is the transformation of a linearly polarized ME dipole into a CP ME dipole; from Ant. 4 to Ant. 6, it is the process of widening ARBW. Fig. 5(a) illustrates the evolution process of the proposed antenna; Fig. 5(b) illustrates the variation in the direction of surface currents and equivalent magnetic currents during the transition from Ant. 1 to Ant. 4; and Figs. 5(c)–(d) present $|S_{11}|$ of different antennas and the maximum achievable ARBW at $\varphi = 0°$.

Ant. 1: Based on the classical linearly polarized ME dipole structure, four identical rectangular patches can be considered as electric dipoles while the current loop that is formed among the four metal rods perpendicular to the ground can be seen as a magnetic dipole. Additionally, the coupled feeding is achieved through the slot on the ground, as shown in Fig. 1(c). The rectangular patches have side lengths of 15.4 mm and 15 mm. Based on the direction of the current, taking $15\,\text{mm} * 2$ gives the length of the electric dipole, which is approximately equal to half-wavelength at the center frequency. IBW of Ant. 1 is 10.7% (4.42 GHz ∼ 4.92 GHz).

Ant. 2: In this step, perturbation elements are introduced to improve the foundation structure to radiate CP waves. Two sets of rectangular patches with different sizes are utilized, namely the main dipole patches and parasitic dipole patches. From Fig. 5(b), it can be observed that there is a presence of transverse current on the patch of Ant. 2, which reduces the angle between the total current and equivalent magnetic current, consequently lowering the AR. This observation is further confirmed in Fig. 5(d). The IBW of Ant. 2 is 11.64% (4.45 GHz ∼ 5 GHz).

Ant. 3: Chamfering the outer edges of one pair of patches, the direction of the total current can be further adjusted, thereby reducing the AR. From Fig. 5(d), it can be observed that the AR of Ant. 3 is lower than that of Ant. 2, but it remains above 3 dB. The IBW of Ant. 3 is 13.61% (4.45 GHz ∼ 5.1 GHz).

TABLE 2. Measured 3 dB ARBW at different frequencies.

f/GHz	$\varphi = 0°$	$\varphi = 90°$
4.78	186° (−123° ∼ 63°)	94° (−58° ∼ 36°)
4.82	248° (−125° ∼ 123°)	115° (−63° ∼ 52°)
4.86	250° (−126° ∼ 124°)	144° (−84° ∼ 60°)

Ant. 4: In this step, a pair of L-shaped branches are added along the edges of the main dipole patches. This configuration allows for the adjustment of current direction and elongates the current path, thereby enhancing resonance at lower frequencies. Similarly, by removing a square portion from the inner side of the parasitic dipole patches, the current direction can be adjusted. From Fig. 5(b), it can be observed that the total current direction of Ant. 4 is parallel to the equivalent magnetic current direction, enabling the radiation of CP waves. From Fig. 5(d), it can be seen that the AR of Ant. 4 is already below 3 dB. From Fig. 5(c), the addition of perturbation elements results in the appearance of three resonance points in the antenna. The coupling of these three resonance points together broadens IBW. The IBW of Ant. 3 is 18.63% with ARBW of 169° ($f = 4.55$ GHz and $\varphi = 0°$).

Ant. 5: Due to the presence of a pronounced right angle in the L-shaped branches of Ant. 4, a discontinuity is introduced. A substantial amount of current converges at the sharp right-angle tip, and a portion of it reflects back. Therefore, chamfering the right angle reduces the discontinuity to ensure a stable phase difference between the two electric field components at large angles, thus improving ARBW. At the end of the L-shaped branches, a pair of VESs are also added, which extends the current path without increasing the antenna size. Furthermore, vertical currents are introduced at the edges of the antenna, which helps to broaden the radiation beam and enhance the phase stability of E_θ and E_φ at large angles. From Fig. 5(c) it can be observed that the third resonance point has risen above −10 dB, resulting in a degradation of IBW. However, from Fig. 5(d), its ARBW has been expanded to 209° ($f = 4.84$ GHz and $\varphi = 0°$). In this step of improvement even small modifications to the L-shaped branches can have a significant impact on the radiation performance, especially on ARBW. This is due to the strong current distribution at the L-shaped branches, as shown in Fig. 6.

Ant. 6: To further enhance ARBW, two other VES structures are also added to the branches of the parasitic dipole patches. Due to the relatively large size of Ant. 5, which is close to $1.0\lambda_L \times 1.0\lambda_L$, efforts are made to miniaturize the antenna by reducing the dimensions of the dielectric substrate and the spacing between the dipoles, resulting in the structure of Ant. 6. Through the structure adjustment and parameter optimization, Ant. 6 exhibits a lower frequency shift in IBW than that of Ant. 5 in Fig. 5(c), achieving an IBW of 18%. Additionally, a significant broadening of ARBW in Fig. 5(d) is achieved in the $\theta > 0°$ region. AR less than 3 dB is achieved within the range of $-119° < \theta < 124°$, resulting in a 243° ARBW ($f = 4.9$ GHz and $\varphi = 0°$). This indicates that the VSE structures contribute significantly to the enhancement of ARBW.

Figure 6 shows the simulated current distributions at different time points within a period at 4.9 GHz of Ant. 6. It can be seen that the direction of the current shows a right-hand CP (RHCP) rotation as time changes.

3. MEASUREMENT RESULT AND DISCUSSION

A fabricated prototype of the designed antenna and its measurement environment are shown in Fig. 7. In a Satimo anechoic chamber, the far-field data are measured at regular intervals of 0.02 GHz during the testing process. In Fig. 8(a), the simulated and measured data of $|S_{11}|$ demonstrate good agreement maintaining a relative IBW of 18%. In Fig. 8(b), the measured minimum AR point is shifted 0.15 GHz lower in frequency than

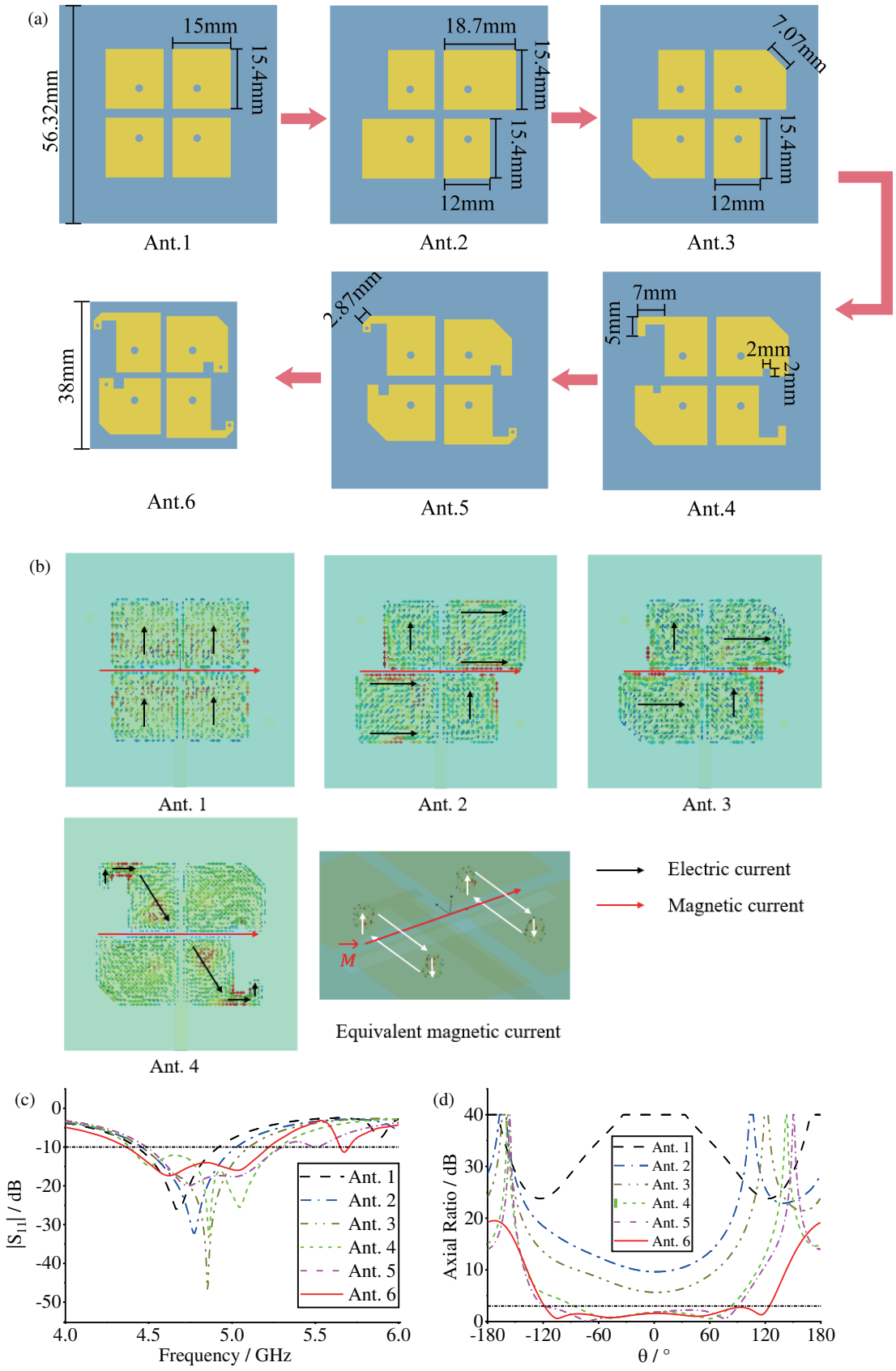

FIGURE 5. Evolution of the antenna. (a) Structures, (b) polarized current orientation diagram (Ant. 1 to Ant. 4) and equivalent magnetic current direction, (c) simulated $|S_{11}|$, and (d) simulated ARBW.

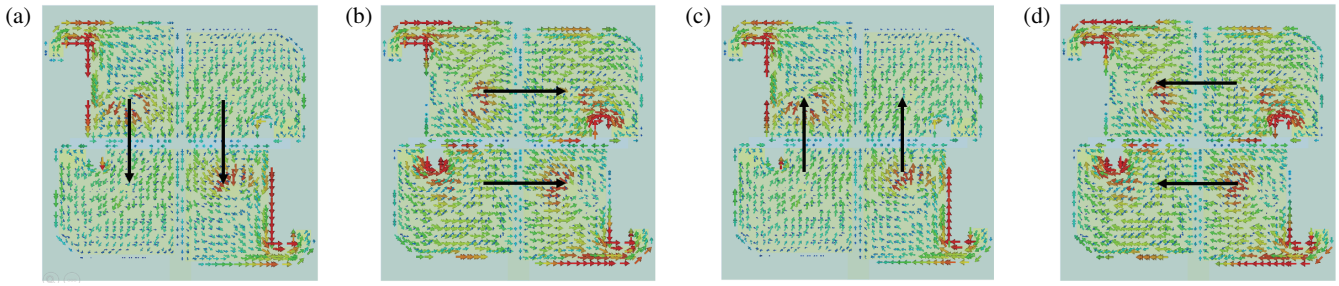

FIGURE 6. Simulated current distributions in different time points within a period at 4.9 GHz. (a) $t = 0$, (b) $t = T/4$, (c) $t = T/2$, and (d) $t = 3T/4$ (T is the period).

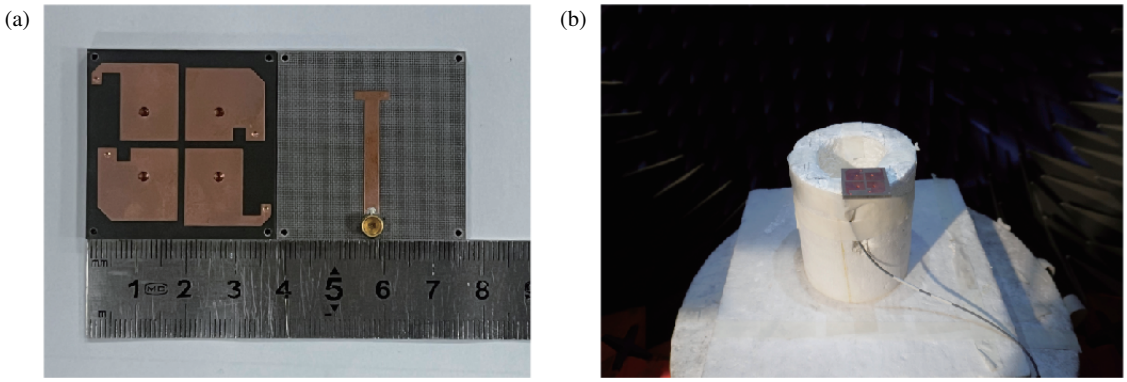

FIGURE 7. Fabrication and measurement of the proposed antenna. (a) Fabricated prototype and (b) measurement environment.

TABLE 3. Comparison between the proposed antenna and recently published wide ARBW CP antennas.

Refs	Feeding	Extra structure	IBW (%)	AR bandwidth (%)	Maximum ARBW (°)	XPD (dB)	Size (λ^3)	Years
[7]	Single port	No	1.7	0.63	188	-	$0.21 \times 0.21 \times 0.016$	2018
[11]	Single port	No	13.8	9	190	33	$0.6 \times 0.6 \times 0.31$	2018
[12]	Single port	No	3.4	0.93	226	17.7	$0.289 \times 0.289 \times 0.013$	2019
[2]	Single port	CBSAs*	18.6	9.5	180	2	$0.7 \times 0.7 \times 0.58$	2021
[5]	Complex SR	Cavity-backed reflector	52.4 (−15 dB)	7.55	254	-	$0.68 \times 0.68 \times 0.18$	2017
[4]	8 ports (dual CP)**	Vertical matal fence	19.3/20.4	8.3/11.3	185/220	-	$0.38 \times 0.38 \times 0.04$	2023
[8]	Complex SR	No	55.6	33	220	15	$1.03 \times 1.03 \times 0.025$	2023
[10]	Complex SR	AMC	18.65	6.25	247	15	$0.91 \times 0.91 \times 0.073$	2023
This work	Single port	No	18	3.34	250	17.4	$0.6 \times 0.6 \times 0.057$	2025

*: Cavity-backed slot antennas (CBSAs).
**: Achieve dual circular polarization by sequentially rotating the feed power to every four ports in one direction.

the simulated one, achieving an AR bandwidth of 3.34% (from 4.71 to 4.88 GHz). The AR bandwidth shift range of the proposed antenna is very small, and it can be easily covered by the bandwidth of the transmitting antenna, without affecting the reception performance of the proposed antenna. The shift in the minimum AR point could be attributed to manufacturing variation or inaccuracy for the L-shaped branches during the fabrication process. Improving machining precision can help resolve this issue in practical applications. Designers can also use tolerance experiments during the design process to assess the potential deviations between simulated results and measured ones arising from machining precision. The variation of ARBW with frequency in the measurement is shown in Table 2. The measured results indicate that at $f = 4.86$ GHz, ARBW reaches its maximum value of 25° on the $\varphi = 0°$ plane, as shown in Fig. 8(c). Here the measured result is in good agreement

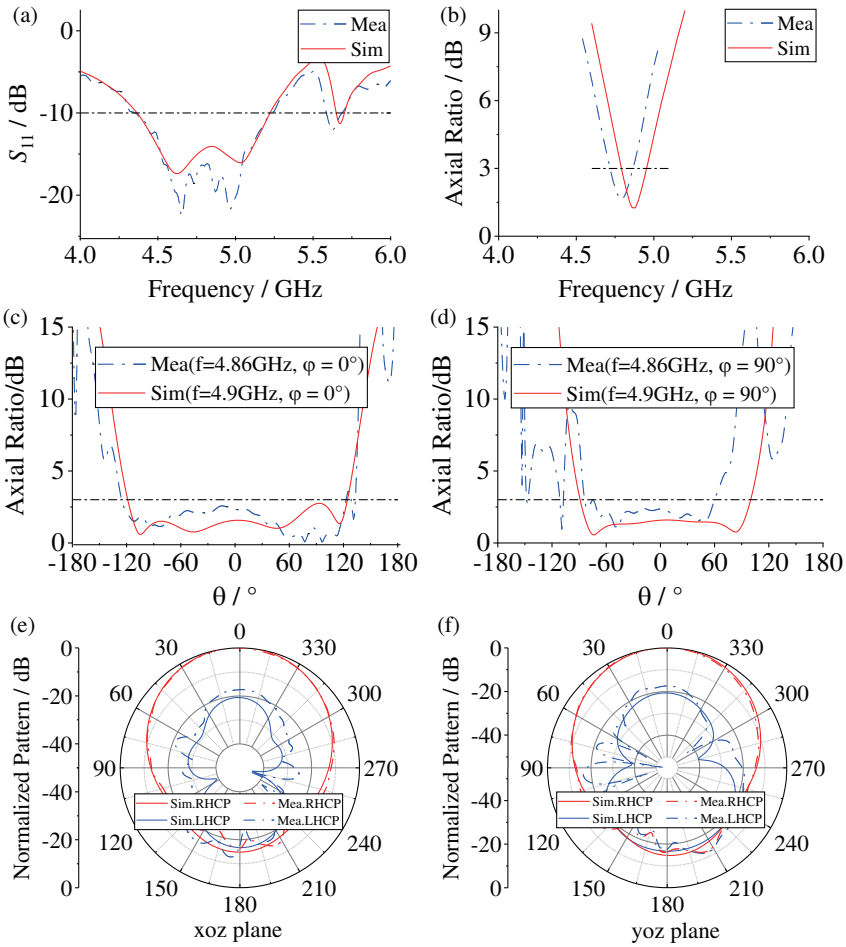

FIGURE 8. Simulated and measured results of the proposed antenna. (a) $|S_{11}|$, (b) AR bandwidth, (c) ARBW in the $\varphi = 0°$ plane, (d) ARBW in the $\varphi = 90°$ plane, (e) normalized radiation pattern in the xoz plane, and (f) normalized radiation pattern in the yoz plane.

with the simulated one. In Fig. 8(d), on the $\varphi = 90°$ plane, ARBW is only 144° at $f = 4.86$ GHz, and this will affect the antenna ability to receive electromagnetic waves at large angles. In addition to machining precision, this discrepancy could also be attributed to the loosening of the adhesive tape that secures the antenna during the rotation of the turntable in the measurement process. As a result, errors may have occurred in the measured AR within the range of $\theta > 0°$. The above result fully demonstrates the capability of the L-shaped branches and VES structures to consistently widen ARBW at $\varphi = 0°$. From Figs. 8(e) and (f), it can be observed that the cross-polarization discrimination (XPD) is 17.4 dB, and the sidelobe level (SLL) is -13.76 dB. The radiating efficiency within the operational bandwidth exceeds 98%, and the gain at $\theta = 0°$ is 6.74 dBi.

Table 3 shows the comparison of the structure and radiation performance between the proposed antenna and other reported ones. To facilitate a better analysis of Table 3, eight comparison references can be divided into two sections: the first four papers [7, 11, 12, 2] focusing on single-feed wide ARBW antennas, and the remaining four papers [4, 5, 8, 10] focusing on multi-feed wide ARBW antennas. Compared with the single-feed microstrip antennas, the antenna proposed in this paper exhibits a significantly wide ARBW and a decent AR bandwidth. The single-feed wide ARBW antenna discussed in [2] is a fully metallic cavity-backed slot antenna. It has a narrower ARBW than the proposed antenna while it shows a wider AR bandwidth. However, its profile spans a thickness of $0.58\lambda_L$, whereas the profile of the proposed antenna is only $0.057\lambda_L$. Compared with the multi-feed wide ARBW antennas, the proposed antenna does not require extra structures to maintain stable spatial phase differences. Moreover, except for [4], the remaining multi-feed wide ARBW antennas necessitate the design of complex SR feeding networks to achieve circular polarization, which results in the significantly larger dimensions than the proposed antenna. Furthermore, ARBW of the proposed antenna is wide compared with those of the other multi-feed antennas. Therefore, although the antenna proposed in this paper sacrifices the operating bandwidth, it offers the following significant advantages: First, it does not require additional cavities or metasurfaces (e.g., AMC) to achieve a wide ARBW. This approach avoids increasing the profile height and raising the complexity of the structure and principles. Second, it eliminates the need for complex feeding networks, greatly reducing the antenna size. Third, it does not require multi-port simultaneous feeding, reducing the number of connectors and further lowering costs. With these advantages, the ARBW of the proposed antenna reaches 250°, surpassing most existing wide ARBW antennas.

4. CONCLUSION

Apart from its AR bandwidth, it is also necessary to consider ARBW of a CP antenna. To address this, we have analyzed the key factors of the stable spatial phase differences that influence ARBW of the CP antenna. Through a decomposed evolution approach, we propose the incorporation of chamfered L-shaped branches and VES structures, which significantly expands ARBW of the CP antenna. In addition, the proposed antenna exhibits a low-profile design and features a simple feeding method, making it well suited for geostationary satellites, GPS systems, etc. Moreover, this method can be used to design antennas with wide ARBW in different frequency bands according to specific requirements.

ACKNOWLEDGEMENT

This work was supported in part by the National Natural Science Foundation of China under Grant 62171093, and in part by the Sichuan Science and Technology Programs under Grants 2023ZYD0013 and 2022JDJQ0032.

REFERENCES

[1] Yang, W. J., Y. M. Pan, and S. Y. Zheng, "A low-profile wideband circularly polarized crossed-dipole antenna with wide axial-ratio and gain beamwidths," *IEEE Transactions on Antennas and Propagation*, Vol. 66, No. 7, 3346–3353, Jul. 2018.

[2] Chen, R.-S., L. Zhu, S.-W. Wong, J.-Y. Lin, Y. Li, L. Zhang, and Y. He, "S-band full-metal circularly polarized cavity-backed slot antenna with wide bandwidth and wide beamwidth," *IEEE Transactions on Antennas and Propagation*, Vol. 69, No. 9, 5963–5968, Sep. 2021.

[3] Yan, Y.-D., Y.-C. Jiao, H.-T. Cheng, and C. Zhang, "A low-profile dual-circularly polarized wide-axial-ratio-beamwidth slot patch antenna with six-port feeding network," *IEEE Antennas and Wireless Propagation Letters*, Vol. 20, No. 12, 2486–2490, Dec. 2021.

[4] Li, X., R. Ma, H. Cai, Y.-M. Pan, and X. Y. Zhang, "High-gain dual-band aperture-shared CP patch antenna with wide AR beamwidth for satellite navigation system," *IEEE Antennas and Wireless Propagation Letters*, Vol. 22, No. 8, 1888–1891, Aug. 2023.

[5] Zheng, D.-Z., Y. Luo, and Q.-X. Chu, "Cavity-backed self-phased circularly polarized multidipole antenna with wide axial-ratio beamwidth," *IEEE Antennas and Wireless Propagation Letters*, Vol. 16, 1998–2001, 2017.

[6] Zhang, X., L. Zhu, and N.-W. Liu, "Pin-loaded circularly-polarized patch antennas with wide 3-dB axial ratio beamwidth," *IEEE Transactions on Antennas and Propagation*, Vol. 65, No. 2, 521–528, Feb. 2017.

[7] Wang, M.-S., X.-Q. Zhu, Y.-X. Guo, and W. Wu, "Compact circularly polarized patch antenna with wide axial-ratio beamwidth," *IEEE Antennas and Wireless Propagation Letters*, Vol. 17, No. 4, 714–718, Apr. 2018.

[8] Xue, H., L. Wu, Z.-L. Xiao, and T.-Y. Hu, "A low-profile broadband circularly polarized patch antenna with wide axial-ratio beamwidth," *IEEE Antennas and Wireless Propagation Letters*, Vol. 22, No. 9, 2115–2119, Sep. 2023.

[9] Liu, S., D. Yang, and J. Pan, "A low-profile circularly polarized metasurface antenna with wide axial-ratio beamwidth," *IEEE Antennas and Wireless Propagation Letters*, Vol. 18, No. 7, 1438–1442, Jul. 2019.

[10] Luo, Y., X. Wang, N. Yan, W. An, and K. Ma, "Low-profile wide axial-ratio beamwidth circularly polarized antenna loaded with artificial magnetic conductor," *IEEE Antennas and Wireless Propagation Letters*, Vol. 23, No. 3, 935–939, 2024.

[11] Al-Saedi, H., W. M. Abdel-Wahab, S. Gigoyan, R. Mittra, and S. Safavi-Naeini, "Ka-band antenna with high circular polarization purity and wide AR beamwidth," *IEEE Antennas and Wireless Propagation Letters*, Vol. 17, No. 9, 1697–1701, Sep. 2018.

[12] Ray, M. K., K. Mandal, and N. Nasimuddin, "Low-profile circularly polarized patch antenna with wide 3 dB beamwidth," *IEEE Antennas and Wireless Propagation Letters*, Vol. 18, No. 12, 2473–2477, Dec. 2019.

[13] Fenn, A., "Theoretical and experimental study of monopole phased array antennas," *IEEE Transactions on Antennas and Propagation*, Vol. 33, No. 10, 1118–1126, Oct. 1985.

[14] Rančić, P. D., J. V. Surutka, and M. I. Kitanović, "The influence of finite ground conductivity on characteristics of a vertical mast (monopole) antenna with elevated feeding," in *EMC'96 ROMA International Symposium on Electromagnetic Compatibility*, 427–432, Rome, Italy, 1996.